Surface Phase Transition of $C_{12}E_1$ at the Air/Water Interface: A Study by Dynamic Surface Tension, External RA FT-IR, and 2D IR Correlation Methods

S. Azizian,*,† K. Shibata, T. Matsuda, T. Takiue, H. Matsubara, and M. Aratono*

Department of Chemistry, Faculty of Sciences, Kyushu University, Hakozaki 6-10-1, Higashiku, Fukuoka 812-8581, Japan

Received: May 29, 2006; In Final Form: July 5, 2006

The surface conformational states of the Gibbs monolayer of ethylene glycol mono-*n*-dodecyl ether ($C_{12}E_1$) at the air/water interface was studied using dynamic surface tension, external reflection−absorption FT-IR spectroscopy (ERA FT-IR), and two-dimensional infrared (2D IR) correlation methods at constant temperature. The dynamic surface tensions were measured at different bulk concentrations of $C_{12}E_1$, and it was observed that a constant surface tension region appears at ~38.5 mN m^{-1} in a dynamic surface tension profile at concentrations higher than 11 μmol kg^{-1}. This constant surface tension region corresponds to the surface phase transition from liquid expanded (LE) to liquid condensed (LC). Two sets of ERA FT-IR spectra were collected, one at different bulk concentrations but after equilibrium time (equilibrium measurements) and another at constant bulk concentration ($m = 16$ μmol kg^{-1}) but at different times (dynamic measurements). The first set of these measurements show that the peak area increases in the range of $11 < m \leq 16$ μmol kg^{-1}, which means the increase in the number of surfactant molecules at the air/water interface. Also, the wavenumber of antisymmetric CH_2 stretching decreases gradually from ~2923 cm^{-1} (for 10 and 11 μmol kg^{-1}) to ~2918 cm^{-1} (for $m \geq 16$ μmol kg^{-1}) with increasing concentration. The wavenumbers of 2923 and 2918 cm^{-1} were assigned to LE and LC phases, respectively, and the decrease of wavenumber in the concentration range of $11 < m \leq 16$ μmol kg^{-1} were correlated to the surface phase transition (LE → LC), or in other words, in the mentioned concentration range, two phases coexist. The dynamic ERA FT-IR measurements at 16 μmol kg^{-1} also confirm the surface phase transition from LE to LC. The 2D IR correlation method was applied to the both equilibrium and dynamic IR spectra of the $C_{12}E_1$ monolayer. The synchronous correlation maps show two strong autopeaks at ~2922 and ~2851 cm^{-1} and also show a strong correlation (cross-peaks) between antisymmetric CH_2 stretching (ν_a) and symmetric CH_2 stretching (ν_s). The asynchronous correlation maps show that both observed bands of ν_a and ν_s in one-dimensional IR split into two components with the characteristic of overlapped bands, which reveals the coexistence of two phases (LE and LC) at the interface at $11 < m \leq 16$ μmol kg^{-1}. The synchronous and asynchronous maps that were obtained from dynamic IR spectra closely resembled the equilibrium map.

Introduction

Adsorbed films (Gibbs monolayers) and insoluble films (Langmuir monolayers) at air/liquid and liquid/liquid interfaces have been studied extensively from both theoretical and practical points of view and also from both thermodynamic and non-thermodynamic aspects. One of the interesting features of Gibbs and Langmuir monolayers is phase transition, which is mainly due to the change in surface density and brought about by the changes in temperature, pressure, and bulk concentration of surfactants in the former and by the compression of the monolayer in the latter. Surface phase transition in Gibbs monolayers has been extensively studied in our laboratory at oil/water[1−5] and air/water[6,7] interfaces from the thermodynamic point of view.

Different techniques such as X-ray diffraction and reflectivity,[5,8] Brewster angle microscopy (BAM),[9,10] sum-frequency vibrational spectroscopy,[11] fluorescence,[12−15] external reflection−absorption FTIR (ERA-FTIR) spectroscopy,[16] and dynamic surface tension measurements[17] can be used to investigate the phase transition at interfaces. Henon and Meunier[9] observed the phase transition of hexadecanoate at the air/water interface by Brewster angle microscopy. Melzer and Vollhardt[10] observed the condensed phase domains of an adsorbed layer of DHBAA by BAM. Recently, Varga et al.[11] reported the gas/liquid phase transition of adsorbed alkyltrimethylammonium alkyl sulfates at the air/water interface by sum-frequency vibrational spectroscopy.

Pollard et al.[15] measured dynamic surface tension of $C_{14}E_1$ at the air/water interface and observed two different plateaus. By using fluorescence microscopy, they confirmed that the plateaus are due to the gas−liquid expanded and liquid expanded−liquid condensed phase transitions, respectively. Recently, Tsay et al.[18] observed two phase transitions (gas−liquid expanded and liquid expanded−liquid condensed) of adsorbed 1-dodecanol at the air/water interface by dynamic surface tension measurements.

One of the most advantageous techniques for studies of monolayers is ERA-FTIR spectroscopy introduced by Dluhy and Cornell.[19] Its theoretical calculation to determine the optimum experimental parameters were developed by Dluhy.[20]

* Corresponding authors. E-mail: sazizian@basu.ac.ir (S.A.); m.arascc@mbox.nc.kyushu-u.ac.jp (M.A.).

† Visiting from the Department of Chemistry, Faculty of Science, Bu-Ali Sina University, Hamadan, Iran.

10.1021/jp063301p CCC: $33.50
Published on Web 08/09/2006

This technique was used by many researchers to study the behavior of a monolayer at air/water interface.[21−29] Among them, Sinnamon et al.[23,24] employed it for investigation of surface phase transition of pentadecanoic acid and also vinyl octadecanoate at the air/water interface.

For studying surface phase transition by ERA-FTIR spectroscopy, it is conceivable with incident polarized light to split the C−H bands into subbands attributable to coexisting phases. However, the limitation of the polarized ERA-FTIR spectroscopy is low signal-to-noise ratio (S/N). To overcome this problem, it is better to employ unpolarized light that has higher S/N but cannot split the bands to subbands and then apply the two-dimensional infrared (2D IR) correlation method to split the bands. The basic concepts of the 2D IR correlation method was proposed by Noda[30] and then developed and used for different systems by Noda and other researchers.[31−41] Elmor and Dluhy[33,34] applied the 2D IR correlation method for the investigation of surface phase transitions in monolayer films at the air/water interface.

Most of the previous studies on surface phase transitions are about Langmuir monolayers of insoluble surfactants, but in the present work, we studied the surface phase transition of Gibbs monolayer of a soluble surfactant that has been less studied. The aim of the present work is to investigate the surface phase transition of the Gibbs monolayer of ethylene glycol mono-*n*-dodecyl ether ($C_{12}E_1$) at the air/water interface at 15 °C by using dynamic surface tension, ERA-FTIR spectroscopy, and the 2D IR correlation method. Aveyard et al. has reported the surface pressure vs area isotherms of $C_{12}E_1$ at both the Langmuir monolayer at air/water interfaces and the Gibbs monolayer at heptane/water interfaces.[42] The phase transition was observed in the Langmuir monolayer, while not observed in the Gibbs one. Although Kato et al. also has reported the phase transition in the Gibbs films of $C_{12}E_1$ at the air/water surface based on dynamic surface pressure and BAM images, their experiments were performed at various temperatures but with different concentrations.[43,44] So, in the present work, we studied this surface phase transition at constant temperature and different concentrations by different methods and from both equilibrium and dynamic points of view.

Materials and Experimental Methods

Materials. Ethylene glycol mono-*n*-dodecyl ether ($CH_3(CH_2)_{11}OCH_2CH_2OH$) (>99%), denoted as $C_{12}E_1$, was purchased from Nikko Chemicals Co. Ltd., Tokyo, Japan. Its purity was confirmed to be more than 99.9% by gas chromatography and thus used as received. Water passed through ion-exchange region was further distilled three times from dilute alkaline permanganate solution.

Dynamic Surface Tension Measurements. The dynamic surface tension was measured by the pendant drop method based on an automatic axisymmetric drop shape analysis[45,46] at constant temperature (15.00 ± 0.01 °C) and at different bulk concentrations of $C_{12}E_1$. The experimental error estimated was within ±0.05 mN m^{-1}.

External Reflection−Absorption FT-IR (ERA-FTIR) Measurements. ERA-FTIR spectra were collected with a Perkin-Elmer (Spectum One) Fourier transform infrared spectrometer equipped with an external reflection attachment (Specac). The mercury−cadmium-telluride (MCT) detector was used by cooling it with liquid nitrogen. The subphase temperature was held constant at 15.00 ± 0.05 °C by flowing thermostated water through the hollow body of the trough. An unpolarized light with the incident angle of 40° was used. For equilibrium and dynamic measurements, all spectra were collected at 4 cm^{-1} resolution by using 1024 and 256 scans, respectively. ERA-FTIR data were reported as $-\log(R/R_o)$, where R_o and R are reflectivities of the pure and film-covered water surfaces, respectively. A two-point baseline correction was applied to the reflectance spectra in the C−H stretching region (without smoothing), then followed by offsetting to the zero absorbance value. For the equilibrium experiments, the reflectance spectra were measured as a function of $C_{12}E_1$ bulk concentration (10−23 μmol kg^{-1}) after 80 min. For the dynamic experiments, the reflectance spectra were measured at 16 μmol kg^{-1} as a function of time, 2, 7, 12, 17, 22, 27, 32, and 38 min after pouring the solution in the IR trough. For both equilibrium and dynamic experiments, the ERA-FTIR measurements were repeated two or three times and the average values were employed. The average errors in measured wavenumbers and calculated peak areas are ±0.9 and ±0.005 cm^{-1}, respectively.

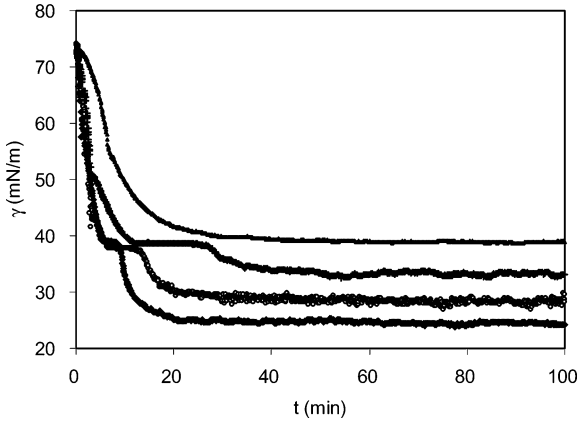

Figure 1. Dynamic surface tension profile of $C_{12}E_1$ adsorption at air/water interface at 15.00 °C and different bulk concentrations. The concentrations are 10, 13, 16, and 20 μmol kg^{-1} from top to bottom.

Calculation of 2D IR Correlation Spectra. The calculations of 2D IR correlation spectra (synchronous and asynchronous) were performed by means of the software provided by professor Ozaki's group as 2Dshige, Shigeaki Morita, Kwansei-Gakuin University (Japan), 2004−2005. The reference spectrum was set equal to zero. For normalization of spectra in mentioned cases, the values of integral intensities, calculated in the range of 2990−2810 cm^{-1}, were chosen as the normalizing factor.[32] In the present study, two kinds of external perturbations were used: concentration and time. In a 2D IR correlation spectrum, the negative cross-peaks were shaded, while the positive peaks were not shaded. In the 2D IR correlation method, when the intensity at two different wavenumbers (ν_1, ν_2) change in the same direction, a positive cross-peak appeared at (ν_1, ν_2) in the synchronous spectrum. A negative cross-peak indicates the opposite. When the spectrum change at ν_1 occurs prior to that at ν_2, then a positive cross-peak appears at (ν_1, ν_2) in the asynchronous spectrum. A negative cross-peak indicates the opposite.

Results and Discussions

Dynamic Surface Tension. We studied the dynamic surface tension at different concentrations and at constant temperature (15.00 °C). Figure 1 shows the dynamic surface tension profiles up to several hours at 10, 13, 16, and 20 μmol kg^{-1}. At all concentrations, an initial plateau appeared at $\gamma \approx 72.4$ mN m^{-1} in a very short time, then the surface tension decreased with time. At concentrations of $m \geq 12$ μmol kg^{-1}, the second plateau appeared around $\gamma \approx 38.5$ mNm^{-1}, and then the surface tension

decreased with time and finally reached the equilibrium value. The second plateau was not observed at concentrations lower that 12 μmol kg^{-1}. These experimental results revealed that the plateaus are shorter and also start earlier at higher bulk concentrations. The presence of a plateau in the dynamic surface tension profile means phase transition in the monolayer.[15,18,47,48] In the present case, the surfactant molecules adsorbed at the air/water interface in the form of gaseous phase (G) and then it seemed to have a very rapid phase transition from the gaseous (G) to the liquid expanded (LE) phase in the first plateau region. After the first plateau, the surface tension decreased rapidly due to further adsorption from the bulk to the interface, then the second plateau around 38.5 mN m^{-1} appeared, which corresponds to another phase transition from the liquid expanded (LE) to the liquid condensed (LC) state.

The second plateau appeared at concentrations of $m \geq 12$ μmol kg^{-1}, and its period decreased with increasing concentration, for example, about 11, 4, and 2 min at 13, 16, and 20 μmol kg^{-1}, respectively. This means that the overall rate of phase transition process increases with increasing concentration. The overall rate may be mainly affected by two steps, one is mainly due to phase transition from LE to LC and another is mainly due to adsorption of surfactant molecules from the bulk to the vacant sites of surface created by the phase transition; it seems that, by increasing the bulk concentration, the rate of surfactant adsorption to the vacant sites increased so that the plateau period decreased. As Figure 1 shows, the time scales for evolution of the covered surface and also equilibrium decreased with increasing bulk concentration. For example, it took about 1.5 and 0.5 h tor reach equilibrium at 10 and 16 μmol kg^{-1}, respectively. This indicates that the concentration gradient drove diffusion from the bulk to the sublayer, which is assumed to be in equilibrium with the adsorbed film, and thus the rate of diffusion increased with increasing bulk concentration. The relation between solubility of nonionic surfactants ($C_{14}E_i$, $i = 1$, 2, and 6) in water and time scales of adsorption and equilibrium have been investigated by Pollard et al., and it was shown that the time scales of adsorption and equilibrium decrease with increasing solubility.[15] Thus the present dynamic surface tension study showed that the phase transition occurs from LE to LC for the $C_{12}E_1$ adsorbed films at $m \geq 12$ μmol kg^{-1} and 15 °C. It should be noted that $C_{12}E_1$ has a small headgroup, and therefore, the hydrocarbon chains of surfactant molecules at the interface can be close to each other so that the attractive van der Waals forces between the chains cause phase transition from LE to LC. For surfactants with large headgroups, such phase transition was not observed because of steric hindrance between the headgroups.[15] Furthermore, because temperature changes the hydration states of surfactant molecules and also the thermal motion of substances, it is one of the parameters that affect the phase transition process.

ERA-FTIR Spectroscopy. For better understanding the monolayer behavior of $C_{12}E_1$, which causes the observed dynamic surface tension pattern mentioned above, the ERA-FTIR technique was applied for studying the surface density and conformational state from both equilibrium and dynamic points of view.

(i) Equilibrium ERA-FTIR. The ERA-FTIR spectra of the C−H stretching vibration region (3000−2800 cm^{-1}) are shown in Figure 2. The spectra were collected at different bulk concentrations of $C_{12}E_1$, ranging from 10 to 23 μmol kg^{-1} (the spectra at 10−16 μmol kg^{-1} were presented in Figure 2). In Figure 2, three bands are clearly observable: the antisymmetric CH_2 stretching band has a peak at $\nu_a^P \sim 2920$ cm^{-1} and is

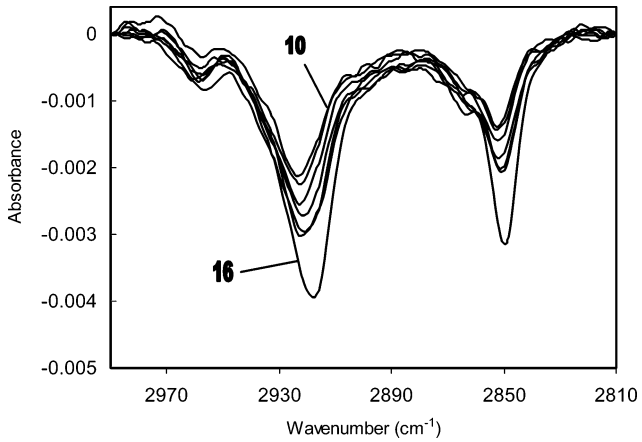

Figure 2. Infrared external reflection−absorption spectra of $C_{12}E_1$ monolayer at air/water interface and at different bulk concentrations with 1 μmol kg^{-1} intervals.

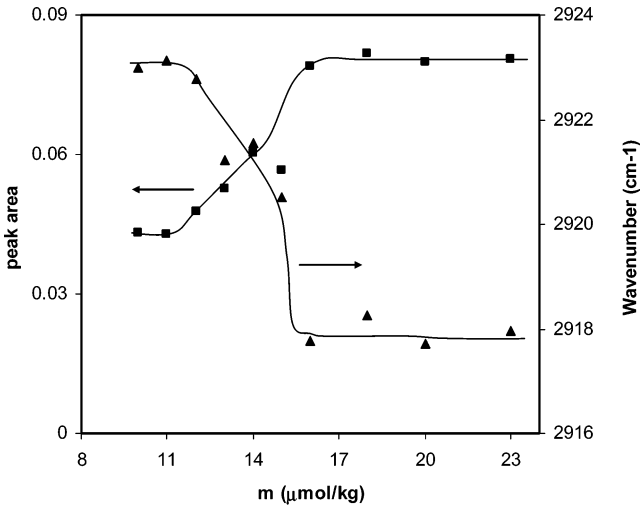

Figure 3. Variation of integrated peak area and wavenumber of antisymmetric CH_2 stretching with bulk concentration of $C_{12}E_1$. The lines are eye guides.

strongest, and the symmetric CH_2 stretching band at $\nu_s^P \sim 2850$ cm^{-1} and the antisymmetric CH_3 stretching band at $\nu_a^P \sim 2960$ cm^{-1}. The intensities of all bands increased with increasing concentration up to 16 μmol kg^{-1}. The variation of the antisymmetric CH_2 stretching band area with concentration is shown in Figure 3. We note that the peak area started to increase around 11 μmol kg^{-1} and remained nearly constant at $m \geq 16$ μmol kg^{-1}. This means that the surface concentration of $C_{12}E_1$ is nearly constant around $m = 10-11$ μmol kg^{-1}, then increases with increasing the bulk concentration in the range of $11 < m \leq 16$ μmol kg^{-1}, and after 16 μmol kg^{-1}, the surface concentration does not change appreciably. However, it should be mentioned here that only a little, often not experimentally detectable, increase in the surface concentration produces a considerable decrease in surface tension in the LC region. Actually, the equilibrium surface tension value of 20 μmol kg^{-1} is considerably lower than that of 16 μmol kg^{-1}, as shown in Figure 1.

Figure 2 shows that the ν_a^P and ν_s^P values of CH_2 shift to the lower ones as the bulk concentration increases. This pattern is visualized for ν_a^P of CH_2 in Figure 3; the wavenumber is constant (~2923 cm^{-1}) at 10 and 11 μmol kg^{-1} but starts to decrease at $m \geq 12$ μmol kg^{-1} up to 16 μmol kg^{-1} and then remains nearly constant (~2918 cm^{-1}) at $m \geq 16$ μmol kg^{-1}. Because the frequencies of CH_2 stretching vibration bands are

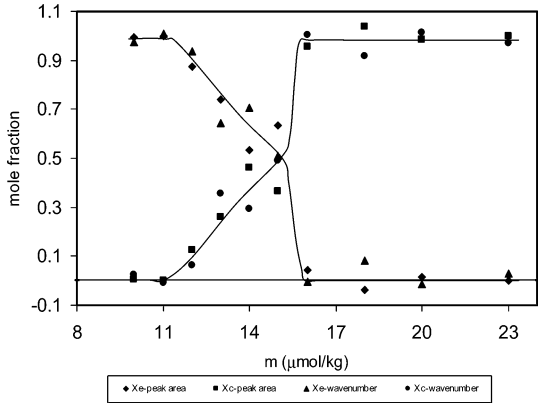

Figure 4. Coverage of LC and LE phases at different bulk concentrations, which was derived by using eqs 1 and 2. The lines are eye guides.

sensitive to the conformational order of the hydrocarbon chain, their shifts to the lower values suggest a disorder-to-order phase transition at the interface. The wavenumbers around ~2923 and ~2917.8 cm^{-1} correspond to the liquid expanded (LE) and liquid condensed (LC) states, respectively.[26] Thus the ERA-FTIR data show that the monolayer of $C_{12}E_1$ has the LE structure at low concentrations ($m \leq 11$ μmol kg^{-1}), and the LC structure at high concentrations ($m \geq 16$ μmol kg^{-1}). At concentrations between 11 and 16 μmol kg^{-1}, the ν_a^P values of CH_2 are between 2923 and 2917.8 cm^{-1}, which may be an indication of the coexistence of the LE and LC phases. The fraction of LE decreases, while that of LC increases with increasing concentration because the ν_a^P is also decreased at $11 < m \leq 16$ μmol kg^{-1}. Therefore, the equilibrium data of ERA-FTIR indicate that the $C_{12}E_1$ monolayer changes its state from the LE phase to the LC phase (surface phase transition) and therefore the hydrocarbon chains become more ordered and close-packed as the bulk concentration increases.

Because the change of absorption spectra in the LE−LC coexistence region is attributable to an superposition of the LE and LC spectra, let us simply assume that neither LE nor LC states changes and only their proportion does in the LE−LC coexistence region, and thus ν_a^P is expressed by an additivity rule in terms of the coverage of LC region X^C as

$$\nu_a^P = (1 - X^C)\nu_a^{P,E} + X^C\nu_a^{P,C} \quad (1)$$

where $\nu_a^{P,E} = 2923$ cm^{-1} and $\nu_a^{P,C} = 2917.8$ cm^{-1}, respectively. Similarly

$$A = (1 - X^C)\,A^E + X^C\,A^C \quad (2)$$

where $A^E = 0.0430$ and $A^C = 0.0805$, respectively. The errors of calculated X^C from the above equations due to experimental errors of ν_a and A are ± 0.17 and ± 0.14, respectively. The X^C values from the two methods have similar values and go up gradually, but steeply near the end of the coexistence region with increasing m, Figure 4.

It should be noted that there is a good agreement between the results of the ERA-FTIR and the dynamic surface tension. Both techniques demonstrated that, at concentrations lower than 12 μmol kg^{-1}, there is not any surface phase transition from LE to LC because there is not any plateau around 38.5 mN m^{-1} in dynamic surface tension profile and also the wavenumbers in ERA-FTIR spectra do not indicate the presence of the LC phase. Thus the ERA-FTIR measurements show the coexistence of LE and LC phases at $11 < m < 16$ μmol kg^{-1} and only the LC phase at $m \geq 16$ μmol kg^{-1}. It should be noted here

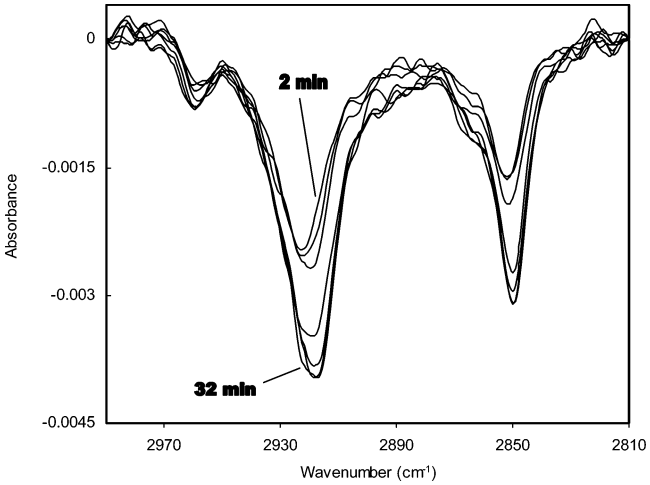

Figure 5. Time dependency of infrared external reflection−absorption spectra of $C_{12}E_1$ monolayer at air/water interface at bulk concentration of 16 μmol kg^{-1} and at 15.00 °C. The time intervals are 5 min.

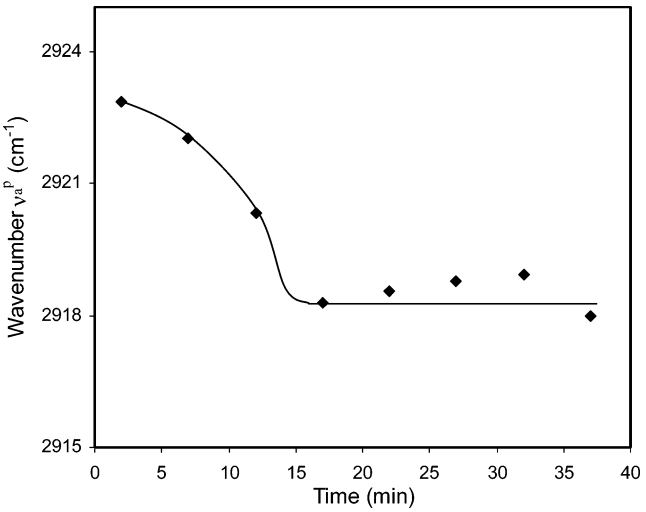

Figure 6. Time dependency of ν_a^P CH_2 stretching wavenumber of $C_{12}E_1$ at air/water interface and at bulk concentration of 16 μmol kg^{-1}. The line is an eye guide.

that this conclusion cannot be drawn only from dynamic surface tension data. The conclusion on the existence of the LC state at high concentrations is in complete agreement with BAM studies.[43,44]

(ii) Dynamic ERA-FTIR. The measurement of the ERA-FTIR as a function of time has been performed in several systems.[25,26,28,29] Figure 5 shows the ERA-FTIR spectra for the C−H stretching region of $C_{12}E_1$ at 16 μmol kg^{-1} and 15.00 ± 0.05 °C that were taken at various times. The value of 16 μmol kg^{-1} was chosen for the dynamic ERA-FTIR studies because its dynamic surface tension profile shows the plateau around 38.5 mN m^{-1} due to the surface phase transition and also its equilibrium ERA-FTIR shows that the surface is finally covered by the LC phase at this concentration. As shown in Figure 5, the intensities of three bands increased with time up to around 20 min and then remained almost constant.

Figure 6 shows the variation of antisymmetric CH_2 stretching wavenumber ν_a^P with time. The wavenumber decreased continuously with time until about 14 min, which means the increase of the fraction of LC states with time. At $t > 17$ min, the wavenumber is nearly constant at around 2918 cm^{-1} and thus the monolayer phase is in the liquid condensed state.

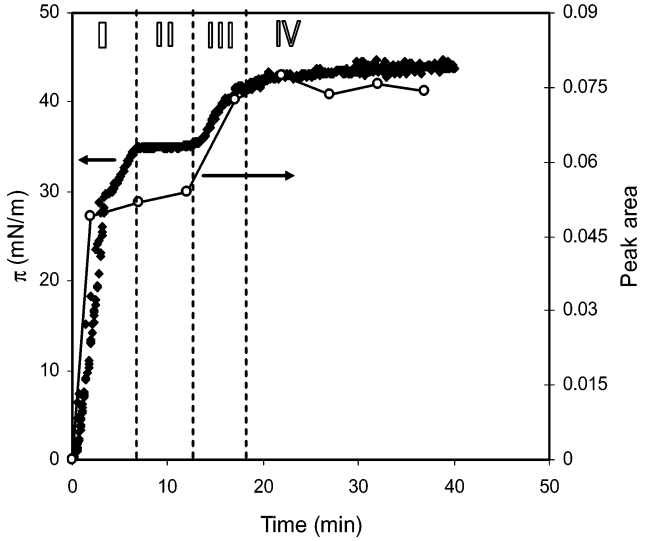

Figure 7. Variation of surface pressure and ν_a CH_2 stretching peak area of $C_{12}E_1$ with time ($m = 16$ μmol kg^{-1}). Filled squares and open circles show surface pressure and IR peak area, respectively.

Figure 7 shows the variation of the peak area of antisymmetric CH_2 stretching and also the surface pressure π ($\pi = \gamma_o - \gamma$) with time at 16 μmol kg^{-1}. It should be noted that the peak area curve is composed of four stages: $t < 7$ min (first stage), $7 < t < 13$ min (second), $13 < t < 19$ min (third), and finally, 19 min $< t$ (fourth).

In the first stage ($t < 7$ min), the surfactant molecules adsorbed rather rapidly onto the air/water interface and the surface was covered by the LE phase at the end of this region. This is proved by the fact that the ν_a^P values of CH_2 is 2923−2922 cm^{-1} in this region. Although the surface may go through the surface phase transition from the gaseous to the LE phase in the earlier stage of this region, this process could not be detected by the ERA-FTIR because this phase transition occurs very fast.

In the second stage ($7 < t < 13$ min), the surface pressure was constant, which corresponds to the surface phase transition from the LE to the LC state, and the peak area is increased only slightly. This suggests that the main process is surface phase transition and maybe the adsorption is a minor process. This conclusion is verified by the fact that the ν_a^P value decreased from ∼2922 to ∼2918 cm^{-1} within the second stage. So, after about 15 min, the surface was covered by the LC phase.

Another interesting region is the third stage ($13 < t < 19$ min) in which both peak area and surface pressure again increased rapidly. The increase in peak area means that the number of adsorbed surfactant molecules increase and therefore the surface pressure should increase too, which is in perfect agreement with the experimental dynamic surface pressure profile. Considering that in this region, the change of ν_a^P value with time is small, as shown in Figure 6, it is concluded that in the third stage, the main process is adsorption and the surface is approaching the LC phase at equilibrium. Finally, in the fourth stage at $t > 19$ min, both peak area and surface pressure are constant at their equilibrium values and the ν_a^P value is also constant within experimental error (∼2918 cm^{-1}, see Figure 6), which indicates that the phase of adsorbed $C_{12}E_1$ is in the equilibrium LC state at a bulk concentration of 16 μmol kg^{-1}.

In summary, the dynamic ERA-FTIR data confirm our views on adsorption and phase transition processes derived from the data of dynamic surface tension. The results and discussions given above for $C_{12}E_1$ at high concentration are in complete agreement with fluorescence microscopy data of $C_{14}E_1$ at high surface pressure.[15]

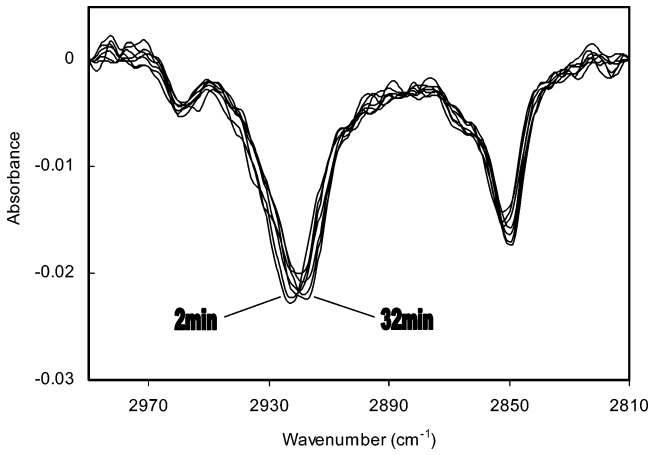

Figure 8. Normalized dynamic external reflection−absorption IR spectra of $C_{12}E_1$ ($m = 16$ μmol kg^{-1}).

2D IR Correlation Analysis. In the previous section on the ERA-FTIR, the surface phase transition and coexistence of the LE and LC phases were suggested on the basis of the change in ν_a^P of CH_2 and the related peak area. The best direct evidence to demonstrate the presence of coexistence phases is to split the antisymmetric CH_2 stretching into two components. Under the unpolarized light in IR spectroscopy, however, this band does not split, and furthermore, the ERA-FTIR peak intensities are so weak that the second derivative and deconvolution methods do not serve, splitting the IR bands. Therefore, for further confidence of coexistence of two phases, we applied the two-dimensional infrared correlation method (2D IR) to the C−H stretching region (2990−2810 cm^{-1}) because this method simplifies the complex spectra consisting of many overlapped peaks and enhances spectra resolution by spreading peaks over the second dimension. In the present study, we used two types of external perturbation form (bulk surfactant concentration and time) and also performed the calculations on both the non-normalized and normalized IR spectra for the 2D IR correlation method. Figure 8 shows an example of the normalized dynamic IR spectra of $C_{12}E_1$ obtained from the spectra in Figure 5.

(i) 2D IR Correlation Method with Concentration Perturbation. A three-dimensional synchronous 2D correlation spectrum was constructed from the normalized concentration dependent IR spectra in the range of 10−16 μmol kg^{-1} and is shown in Figure 9; also, its contour plot is shown in Figure 10a. It is seen that two big autopeaks appear in the diagonal positions at ∼2922 and ∼2851 cm^{-1}, which were assigned to ν_a^P and ν_s^P of CH_2, respectively. Two strong positive cross-peaks appear at off-diagonal positions (2922, 2851 cm^{-1} and 2851, 2922 cm^{-1}, respectively) and form the correlation square with two autopeaks. This indicates that two separate peaks at $\nu_a^P \sim 2922$ and $\nu_s^P \sim 2851$ cm^{-1} have a correlation that their intensities change to the same direction as the bulk concentration changes. There are also four weak positive cross-peaks (2958, 2922 cm^{-1}, 2958, 2851 cm^{-1}, 2851, 2958 cm^{-1}, and 2922, 2958 cm^{-1}). On the basis of the presence of these four weak and positive cross-peaks, it is concluded that there is a weak autopeak at ∼2958 cm^{-1}, which was assigned to the ν_a^P of CH_3. Therefore, the intensities at 2851, 2922, and 2958 cm^{-1} change to the same direction with the concentration perturbation. This finding in Figures 9 and 10a is in agreement with one-dimensional ERA-FTIR spectra in Figure 2.

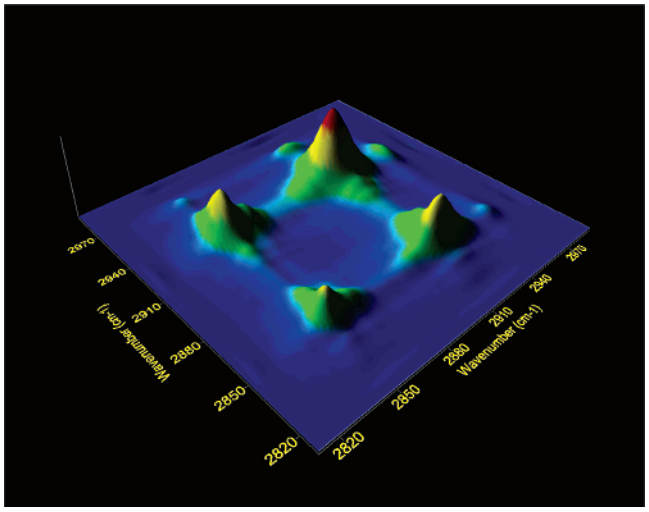

Figure 9. Three-dimensional representation of synchronous two-dimensional IR correlation spectra of $C_{12}E_1$ at air/water interface that are constructed by concentration perturbation and normalized data.

The asynchronous 2D correlation spectrum in the concentration range of 10−16 μmol kg^{-1} from normalized one-dimensional ERA-FTIR spectra is illustrated in Figure 10b. The spectra demonstrate clearly that both bands at $\nu_a^P \sim 2922$ and $\nu_s^P \sim 2851$ cm^{-1} of CH_2 in the synchronous spectrum, respectively, have a significant overlap and each of them can be separated into two bands at about 2926 and 2915 cm^{-1} for ν_a^P and about 2854 and 2848 cm^{-1} for ν_s^P, respectively. These values of wavenumbers after the separation are very close to the reported values from asynchronous spectra for DPPC at air/water interface.[37] The cross-peaks at 2926 and 2915 cm^{-1} and also those at 2854 and 2848 cm^{-1} reveal the coexistence of disordered and ordered conformational states of adsorbed layer, respectively. Another interesting data from the asynchronous spectrum is that the cross-peak at 2926 and 2915 cm^{-1} is positive while the one at 2915 and 2926 cm^{-1} is negative. This means that the band at 2926 cm^{-1} of the disordered phase changes before the band at 2915 cm^{-1} of the ordered phase; in other words, at first the intensity of the disordered phase starts to decrease and then that of the ordered phase starts to increase. This process confirms the surface phase transition from the disordered to the ordered phase by increasing $C_{12}E_1$ concentration. The same behavior was observed for cross-peaks at 2854 and 2848 cm^{-1} and 2848 and 2854 cm^{-1}.

The 2D IR synchronous and asynchronous spectra were also constructed from the concentration dependence of original (not normalized) one-dimensional IR spectra in the range of 10−16 μmol kg^{-1} and gave essentially the same results as those given in Figure 10a and b.

Here it should be mentioned that the reason for the appearance of cross-peaks near the diagonal in the asynchronous spectrum is either the coexistence of two overlapped subbands or a simple frequency shift of one IR band. The computer simulations showed that, in the case of "overlapped peaks", the correlation cross-peaks in an asynchronous spectrum are doublet, one of them is positive and another negative, and the peaks are not elongated along the diagonal, while in the case of "frequency shifting", the cross-peaks are quartet, two of them are positive and the others negative, and the peaks are elongated along the diagonal.[31,33,34] In the present study, the cross-peaks in Figure 10b resemble the simulated spectra for the "overlapped peaks" model. Therefore, it is concluded that the bands of symmetric and antisymmetric CH_2 stretching for $C_{12}E_1$ at the air/water interface consist of two overlapped peaks.

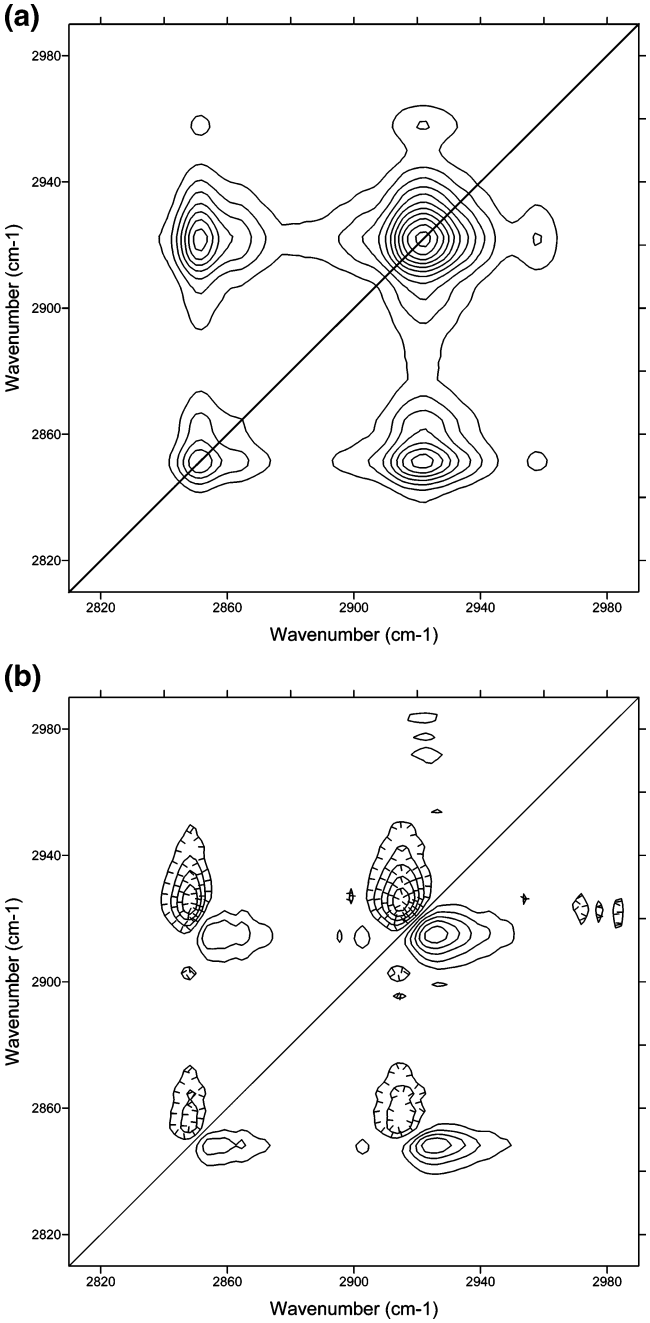

Figure 10. (a) Contour map of synchronous 2D IR correlation spectra of $C_{12}E_1$ at air/water interface that are constructed by concentration perturbation and normalized data. (b) Contour map of asynchronous 2D IR correlation spectra of $C_{12}E_1$ at air/water interface that are constructed by concentration perturbation and normalized data.

Thus the 2D IR correlation spectra obtained on the basis of concentration perturbation for $C_{12}E_1$ show that the antisymmetric CH_2 stretching band includes two overlapping subbands, where one of them increases with increasing concentration while the other decreases. These two subbands correspond to the disordered and ordered phases at the interface and disclosed the surface phase transition being invisible in the original one-dimensional IR, which is in agreement with the conclusion derived from the profile of dynamic surface tension versus time (coexistence of two phases) and that of the ν_a^P of CH_2 versus bulk concentration.

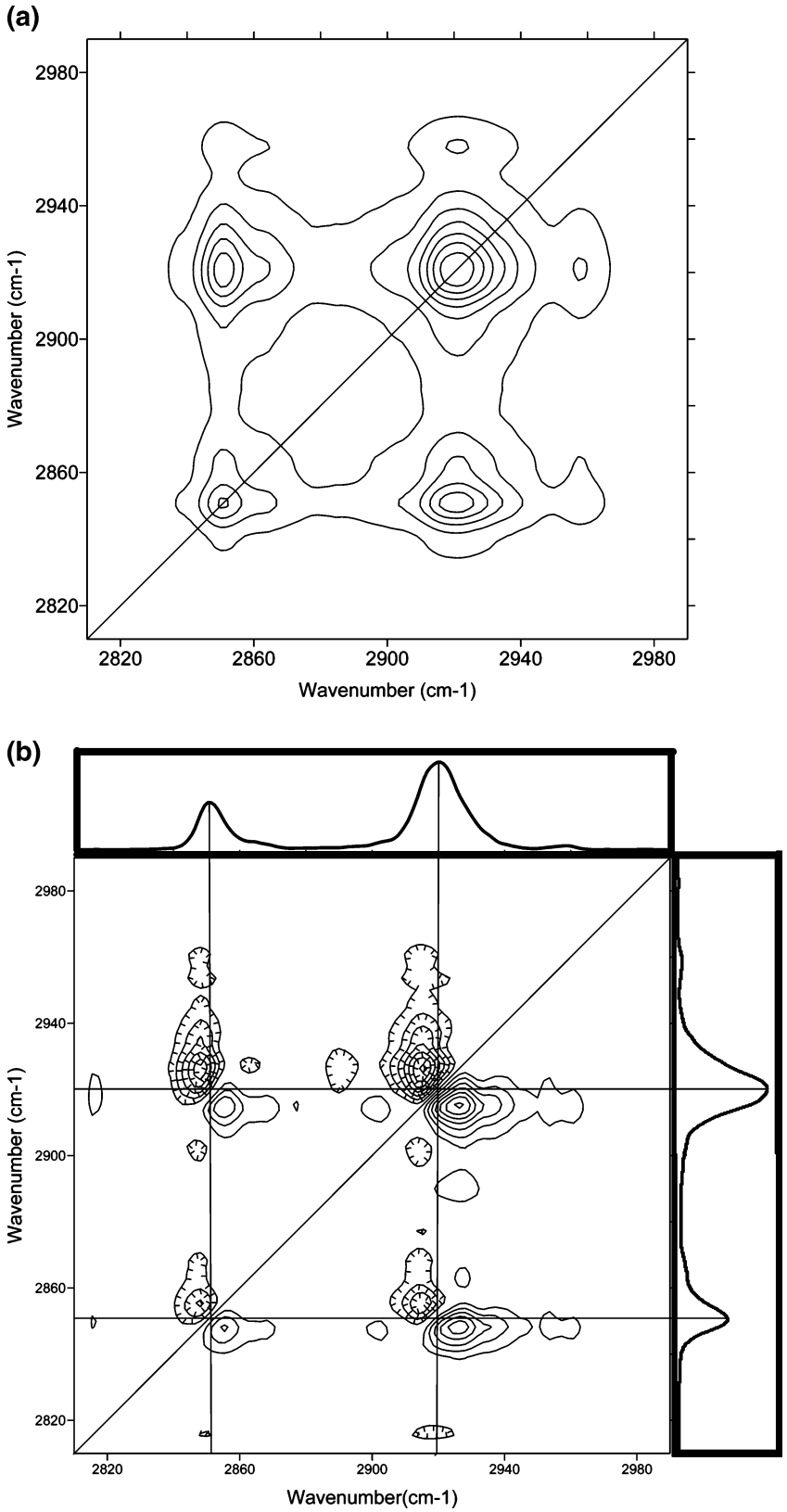

Figure 11. (a) Contour map of synchronous 2D IR correlation spectra of $C_{12}E_1$ at air/water interface that are constructed by time perturbation and normalized data. (b) Contour map of asynchronous 2D IR correlation spectra of $C_{12}E_1$ at air/water interface that are constructed by time perturbation and normalized data.

(ii) 2D IR Correlation Method with Time Perturbation. For further confirmation of the results in (*i*), 2D IR correlation was calculated by using the time-dependent IR spectra given in Figures 5 and 8 in the range of 2−32 min for $m = 16$ μmol kg^{-1}. The contour plots of synchronous and asynchronous spectra obtained from the normalized data given in Figure 8 are shown in Figure 11a and b, respectively. The synchronous plot again shows the strong autopeaks at 2922 and 2851 cm^{-1}

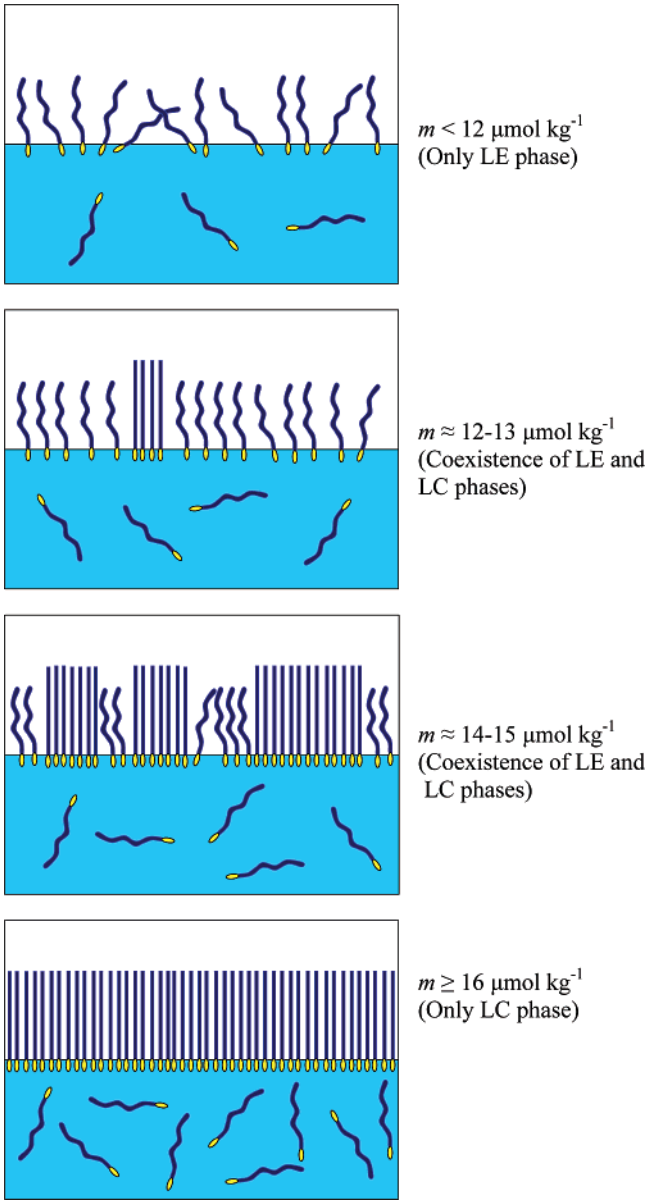

Figure 12. Cartoon presentation of different phases of $C_{12}E_1$ monolayer at air/water interface and at different bulk concentrations.

for ν_a and ν_s of CH_2 and also strong correlation (cross-peaks) between them, which are in perfect agreement with the results of the concentration perturbation synchronous plot (Figure 10a).

The asynchronous plot in Figure 11b shows the splitting of 2922 and 2851 cm^{-1} bands into two subbands corresponding to the disordered and ordered surface phases. The signs of cross-peaks at the asynchronous plot (Figure 11b) show that by changing of time, the subband of the disordered phase starts to decrease and then the subband of ordered phase starts to increase, which shows the surface phase transition takes place from the disordered to the ordered phase as time passes. Again, there is a perfect agreement of the results of asynchronous plots between the concentration and time perturbation methods. The synchronous and asynchronous spectra (not shown here) obtained from the nonnormalized data of dynamic one-dimensional IR spectra (Figure 5) were very similar to those from the normalized data (Figure 11a, b).

In summary, the 2D IR correlation results from the concentration and also the time perturbation methods both for the normalized and nonnormalized input data show that the changes in ν_a^p and ν_s^p of CH_2 in the ERA-FTIR spectra are due to the changes in intensities of the two overlapping bands, which correspond to the disordered (LE) and ordered (LC) phases. The results of all three methods of dynamic surface tension, external RA FT-IR, and 2D IR correlation confirm the presence of coexisting phases (LE and LC) and also surface phase transition for $C_{12}E_1$ at the air/water interface.

Conclusion

The dynamic surface tension profile of $C_{12}E_1$ at air/water interface at 15.00 °C showed a plateau around 38.5 mN m^{-1}, which means that there is surface phase transition from LE to LC. This surface phase transition appears at bulk concentrations higher than 11 μmol kg^{-1}. The overall rate of surface phase transition increased with increasing of bulk concentration due to the increase of adsorption rate to the vacant sites. On the basis of wavenumbers of the C−H stretching region and its variation with concentration measured by ERA FT-IR at equilibrium, it is concluded that, at $m \leq 11$ μmol kg^{-1}, the surface phase is LE, while at $m \geq 16$ μmol kg^{-1}, it is LC. In the concentration range of $11 < m < 16$ μmol kg^{-1}, the LE and LC phases coexist. The peak area of CH_2 stretching showed a considerable increase at the bulk concentration range of $11 < m \leq 16$ μmol kg^{-1}, which means that the number of surfactant molecules increased considerably at interface in the mentioned bulk concentration range. So it is concluded that, in the concentration range of $11 < m \leq 16$ μmol kg^{-1}, a surface phase transition from disordered to the ordered and close packed structure occurs, and therefore, some vacant sites appear at the interface and $C_{12}E_1$ molecules adsorb to these vacant sites (as a result, the peak area increases). This conclusion is in perfect agreement with wavenumber changes and also dynamic surface tension profiles. Figure 12 shows a schematic illustration of surface phase behavior of $C_{12}E_1$ at the air/water interface and at different bulk concentrations, which has been constructed on the basis of the results of the present study. The dynamic ERA FT-IR data confirm the LE to LC phase transition. The synchronous plots of 2D IR which were constructed by the concentration perturbation method show two strong autopeaks for ν_a and ν_s CH_2 stretching and also show positive cross-peaks, which reveal the similarities in the direction of autopeak intensity variation. The asynchronous plot of the 2D IR method shows the pattern of overlapped peaks, so it was found that the CH_2 stretching band in one-dimensional IR consists of two peaks at which their wavenumbers correspond to the disordered and ordered phases. The sign of cross-peaks at asynchronous plots indicate that the disordered phase converts to the ordered phase, i.e., the surface phase transition of $C_{12}E_1$ at air/water interface. The synchronous and asynchronous plots of 2D IR that were constructed by time perturbation method are in complete agreement with concentration perturbation data. Finally, the 2D IR correlation data support the interpretations that were obtained from external RA FT-IR and dynamic surface tension methods.

Acknowledgment. S. Azizian acknowledges support from the Japan Society for Promotion of Science (JSPS) for providing a postdoctoral fellowship (no. P 05137) at Kyushu University. This work was supported in part by the Grant-in-Aid for Scientific Research (B) (no. 1635005).

References and Notes

(1) Matubayashi, N,; Motomura, K.; Aratono, M.; Matuura, R. *Bull. Chem. Soc. Jpn.* **1978,** *51*, 2800.

(2) Takiue, T.; Uemura, A.; Ikeda, N.; Motomura, K.; Aratono, M. *J. Phys. Chem.* **1998**, *102*, 3724.
(3) Takiue, T.; Matsuo, T.; Ikeda, N.; Motomura, K.; Aratono, M. *J. Phys. Chem.* **1998**, *102*, 4906.
(4) Aratono, M.; Takiue, T. *Encycl. Surf. Colloid Sci.* **2002**, 3098 and references therein.
(5) Pingali, S.; Takiue, T.; Luo, G.; Tikhonov, M.; Ikeda, N.; Aratono, M.; Schlossman, M. *J. Phys. Chem. B* **2005**, *109*, 1210.
(6) Aratono, M.; Uryu, S.; Hayami, Y.; Motomura, K.; Matuura, R. *J. Colloid Interface Sci.* **1983**, *93*, 162.
(7) Aratono, M.; Uryu, S.; Hayami, Y.; Motomura, K.; Matuura, R. *J. Colloid Interface Sci.* **1984**, *98*, 33.
(8) Pershan, P. S. *Faraday Discuss.* **1990**, *89*, 231.
(9) Henon, S.; Meunier, J. *J. Chem. Phys.* **1993**, *98*, 9148.
(10) Melzer, V.; Vollhardt, D. *Phys. Rev. Lett.* **1996**, *76*, 3770.
(11) Varga, I.; Keszthelyi, T.; Meszaros, R.; Hakkel, O.; Gilanyi, T. *J. Phys. Chem. B* **2005**, *109*, 872.
(12) Losche, M.; Mohwald, H.; *Rev. Sci. Instrum.* **1984**, *55*, 1968.
(13) Kmobler, C. M. *Science* **1990**, *249*, 870.
(14) Truskett, V. N.; Stebe, K. J.; *Langmuir* **2003**, *19*, 8271.
(15) Pollard, L. M.; Pan, R.; Steiner, C.; Maldarelli, C. *Langmuir* **1998**, *14*, 7222.
(16) Mendelsohn, R.; Brauner, J. W.; Gericke, A. *Annu. Rev. Phys. Chem.* **1995**, *46*, 305.
(17) Vollhardt, D.; Fainerman, V. B.; Emrich, G. *J. Phys. Chem. B* **2000**, *104*, 8536.
(18) Tsay, R.-Y.; Wu, T.-F.; Lin, S.-Y. *J. Phys. Chem. B* **2004**, *108*, 18623.
(19) Dluhy, R. A.; Cornell, D. G. *J. Phys. Chem.* **1985**, *89*, 3195.
(20) Dluhy, R. A. *J. Phys. Chem.* **1986**, *90*, 1373.
(21) Dluhy, R.; Ping, Z.; Faucher, K.; Brockman, J. M. *Thin Solid Films* **1998**, *327*, 308.
(22) Kawai, T.; Kamio, H.; Kon-No, K. *Langmuir* **1998**, *14*, 4964.
(23) Sinnamon, B. F.; Dluhy, R.; Branes, G. T. *Colloids Surf., A* **1999**, *146*, 49.
(24) Sinnamon, B. F.; Dluhy, R.; Branes, G. T. *Colloids Surf., A* **1999**, *156*, 215.
(25) Wen, X.; Lauterbach, J.; Franses, E. I. *Langmuir* **2000**, *16*, 6987.
(26) Wen, X.; Franses, E. I. *Langmuir* **2001**, *17*, 3194.
(27) Campbell, R. A.; Parker, S. R. W.; Day, J. P. R.; Bain, C. D. *Langmuir* **2004**, *20*, 8740.
(28) Meister, A.; Kerth, A.; Blume, A. *J. Phys. Chem. B* **2005**, *109*, 6239.
(29) Kim, S. H.; Franses, E. I. *J. Colloid Interface Sci.* **2006**, *295*, 84.
(30) Noda, I. *J. Am. Chem. Soc.* **1989**, *111*, 8116.
(31) Gericke, A.; Gadaleta, S. J.; Brauner, J. W.; Mendelsohn, R. *Biospectroscopy* **1996**, *2*, 341.
(32) Czarnik-Matusewicz, B.; Murayama, K.; Wu, Y.; Ozaki, Y. *J. Phys. Chem. B* **2000**, *104*, 7803.
(33) Elmore, D. L.; Dluhy, R. A. *Colloid Surf., A* **2000**, *171*, 225.
(34) Elmore, D. L.; Dluhy, R. A. *Appl. Spectrosc.* **2000**, *54*, 956.
(35) Berry, R. J.; Ozaki, Y. *Appl. Spectrosc.* **2001**, *55*, 1092.
(36) Tee, E. M.; Awichi, A.; Zhao, W. *J. Phys. Chem. A* **2002**, *106*, 6714.
(37) Elmore, D. L.; Shanmukh, S.; Dluhy, R. A. *J. Phys. Chem. A* **2002**, *106*, 3420.
(38) Shanmukh, S.; Dluhy, R. A. *J. Phys. Chem. B* **2004**, *108*, 5625.
(39) Noda, I. *Vib. Spectrosc.* **2004**, *36*, 143 and references therein.
(40) Padermshoke, A.; Sato, H.; Katsumoto, Y.; Ekgasit, S.; Noda, I.; Ozaki, Y. *Polymer* **2004**, *45*, 7159.
(41) Yamaghuchi, Y.; Nge, T. T.; Takemura, A.; Hori, N.; Ono, H. *Biomacromolecules* **2005**, *6*, 1941.
(42) Aveyard, R.; Carr, E.; Slezok, H. *Can. J. Chem.* **1985**, *63*, 2742.
(43) Islam, M. N.; Kato, T. *J. Phys. Chem. B* **2003**, *107*, 965.
(44) Islam, M. N.; Kato, T. *J. Colloid Interface Sci.* **2005**, *289*, 581.
(45) Murakami, R.; Sakamoto, H.; Hayami, Y.; Matsubara, H.; Takiue, T.; Aratono, M. *J. Colloid Interface Sci.* **2006**, *295*, 209.
(46) Sakamoto, H.; Murao, A.; Hayami, Y. *Inst. Image Inf. Television Eng. Jpn.* **2002**, *56*, 1643.
(47) Subramanyam, R.; Maldarelli, C. *J. Colloid Interface Sci.* **2002**, *253*, 377.
(48) Melzer, V.; Vollhardt, D.; Weidemann, G.; Brezesinski, G.; Wagner, R.; Mohwald, H. *Phys. Rev. E* **1998**, *57*, 901.